

Optimal Sensorless Four Switch Direct Power Control of BLDC Motor

S. Hajiaghahi^{*}, Z. Rafiee, A. Salemnia, M.R. Aghamohammadi

Department of Electrical Engineering, Shahid Beheshti University, Tehran, Iran.

Abstract- Brushless DC (BLDC) motors are used in a wide range of applications due to their high efficiency and high power density. In this paper, sensorless four-switch direct power control (DPC) method with the sector to sector commutations ripple minimization for BLDC motor control is proposed. The main features of the proposed DPC method are: (1) fast dynamic response (2) easy implementation (3) use of power feedback for motor control that is much easy to implement (4) eliminating the torque dips during sector-to sector commutations. For controlling the motor speed, a position sensorless method is used enhancing drive reliability. For reference speed tracking, a PI control is also designed and tuned based on imperialist competition algorithm (ICA) that reduces reference tracking error. The feasibility of the proposed control method is developed and analyzed by MATLAB/SIMULINK[®]. Simulation results prove high performance exhibited by the proposed DPC strategy.

Keyword: Brushless DC motor; Direct power control ; Four-switch inverter; Sensorless ; Torque ripple..

NOMENCLATURE

BLDC	Brushless direct current
DPC	Direct power control
DTC	Direct torque control
EMF	Electromotive force
ICA	Imperialist competition algorithm
PWM	Pulse width modulation
SVM	Space vector modulation

1. INTRODUCTION

BLDC motors have many advantages including easy control, low maintenance, high efficiency, better speed versus torque characteristics, high dynamic response, reduced weight, and more compact construction. Due to their favorable electrical and mechanical features, BLDC motors are widely used in aerospace, military, automotive applications, industrial and household products [1]–[3]. Consequently, many studies have been developed to enhance the performance of BLDC motors [4]–[6]. Various control strategies for BLDC motors have been proposed in Ref. [7]. Most common methods are based on dc link current control, direct torque control (DTC) in Ref. [8], and space vector control.

Most of the presented methods for power control of

BLDC motors are based on current control and use PI controllers or hysteresis current regulators as internal loops. An alternative six-switch converter strategy to control the mutual torque production through an active and reactive rotor power control loop is presented in Ref. [9] which rotor orientation or back-EMF harmonic content estimation don't require. In Ref. [10] the balance between commutation torque ripple minimization and loss optimization simultaneously by controlling the motor operation in hybrid two- and three-phase conduction is proposed. The six-switch proposed method leads to motor operation in three-phase conduction during overlap area and in two-phase conduction during non-overlap area.

For controlling BLDC motor, an inverter should be used. The inverter switches are not ideal and have switching and conducting losses which reduce the efficiency of the drive. Reducing the number of switches in inverters or using high-performance processors can minimize these losses [6],[7]. In general, BLDC motors are excited by six-switch converter which produce six commutation sequences. However, a low-cost drive system is an important issue in the design and development of modern motor control drives. Hence, for decreasing the switching losses in Ref. [4] a DTC technique for BLDC motors with non-sinusoidal back electromotive force (EMF), using a four-switch converter in the constant torque region is presented. This approach propose a two-phase conduction mode, unlike conventional six-step current and voltage control schemes, by proper selection of the voltage space vectors of the inverter from a simple look-up table at a

Received: 04 June. 2018

Revised: 27 August. 2018

Accepted: 09 December. 2018

*Corresponding author: S. Hajiaghahi

E-mail: S_Hajiaghahi@sbu.ac.ir

Digital object identifier: 10.22098/joape.2019.4859.1374

Research Paper

©2019 University of Mohaghegh Ardabili. All rights reserved.

predefined sampling time, the desired quasi-square wave current is obtained. Four-switch converter controlled by the current PWM control strategy has been proposed in Ref. [13]. Current distortion in the two-phase causes by back-EMF of silent phase and generating 120° conducting current in the three-phase winding of BLDC motor by four-switch converter are main problems of the proposed technique. Four-switch three-phase inverter controlled by digital signal controller which combines the features of microcontroller and digital signal processor on a single chip for BLDC motor is proposed in Ref. [14]. Difficulty in generation constant output torque for Back-EMF trapezoidal shape with 120° conduction and 60° non-conducting regions and the quasi-square wave currents is a main problem of the mentioned method. In Ref. [15], four-switch three-phase converter controlled by direct power control method using a PI controller for BLDC motor is presented.

BLDC motors require an inverter and a rotor position sensor to perform commutation process but applying a sensor on the motor shaft causes operation limit in high speeds. According to position sensor sensitivity, high mechanical vibration and heat produced by motor operation cause an error on measured position value. Moreover, the position sensor has several disadvantages such as increasing machine size, drive's cost, noise immunity and reliability. These problems have caused to use estimation strategies of position such as the open phase current sensing strategy; this technique to estimate uses the conducting interval of freewheeling diodes connected in antiparallel with power transistors [16]. In Refs. [17], [18] the third harmonic of back-EMF is proposed, this technique removes the fundamental harmonic and other poly phase components through a simple summation of three-phase voltages. The back-EMF integrating method is presented in Ref. [19], the principle integration is constant from Zero Crossing Point to 30° . In Ref. [20] the open phase voltage sensing method is proposed. In this paper, used proposed sensorless control method estimates the rotor position by a trapezoidal back-EMF of BLDC motors and uses an unknown input observer for measuring the back-EMF of the BLDC motor in Ref. [21].

Another disadvantage of BLDC motors is the high torque ripple. For reducing commutation torque ripple, several strategies have been proposed for intense, a novel switching pattern incorporating with the voltage vector look-up table in two-phase conduction mode has been designed in order to regulate controllable phases torques in Ref. [22]. A novel boost front end without

extra inductors has been proposed in Ref. [23], the boost front end could boost the capacitor voltage with the motor stator inductances, thus decreases the effect of the DC-link voltage on commutation torque ripple reduction to a large extent. A combination of a three-level diode-clamped multilevel inverter, a modified single-ended primary-inductor converter, and a DC-link voltage selector circuit is employed for torque ripple suppression circuit [24]. For effectively reducing the torque pulsation, the DC-link voltage selector circuit is used to apply the regulated DC-link voltage from the modified single-ended primary-inductor converter during the commutation interval. Also, commutation torque ripple reduction in three-phase four-switch inverter-fed motor drives is proposed in Refs. [25], [26]. DPC is a control method in which is directly selected output voltage vector states based on the power and flux fluctuations using hysteresis controllers and without using current loop. In this respect, it is similar to the well know DTC strategy. DPC strategy has many of advantages of DTC such as fast dynamic and ease of implementation and hasn't any DTC's problems [27], [28]. In DTC, real torque measurement is variable in practice. The feedback of torque control, because it is estimated by the algorithm to be exclusive, so it is vulnerable to many factors, including model accuracy, parameter change, and so on. However, in DPC, it is easy to measure the actual values of the control variables by measuring the voltage and current in a real system therefore, this paper proposes four-switch inverter controlled by PWM scheme using an optimum PI controller for BLDC motor. Four-switch topology reduces the cost of drive because it decreases the number of the switch. Also, in this paper, by eliminating position sensors and using feasible sensorless strategy, cost of a BLDC motor drive can be more reduced.

The main contributions of the paper are listed below: 1) this paper proposed four-switch sensorless DPC control of BLDC motor with commutation ripple minimization which has not been done in previous research 2) a new method to sector to sector communication torque ripple minimization for four-switch DPC is proposed 3) tuning PI controller to reduce error tracking speed reference by ICA algorithm 4) using the sensorless method and four-switch inverter reduces the cost and volume of the drive and increases system reliability. This paper is organized as follows. Section 2 points out necessary equations related to the mathematical modeling of BLDC motor. Section 3 explains the proposed four-switch DPC method for BLDC drive. MATLAB/SIMULINK[®] software based simulation studies are presented in section 4.

Conclusion is given in section 5.

2. THREE PHASE BLDC MOTOR MODELING

This BLDC motors with trapezoidal back-EMFs are suitably fed by 120° rectangular shaped currents that should be synchronized with the back-EMFs in order to develop a constant electromagnetic torque in which ripple is reduced. The mathematical expression of a three-phase BLDC motor can be shown as [29]

$$\begin{bmatrix} V_a \\ V_b \\ V_c \end{bmatrix} = \begin{bmatrix} r & 0 & 0 \\ 0 & r & 0 \\ 0 & 0 & r \end{bmatrix} \times \begin{bmatrix} i_a \\ i_b \\ i_c \end{bmatrix} + \begin{bmatrix} L_s - M & 0 & 0 \\ 0 & L_s - M & 0 \\ 0 & 0 & L_s - M \end{bmatrix} \frac{d}{dt} \begin{bmatrix} i_a \\ i_b \\ i_c \end{bmatrix} + \begin{bmatrix} E_a \\ E_b \\ E_c \end{bmatrix} \quad (1)$$

where V_x , i_x , and E_x are voltage, back-EMF and current of the stator winding for each phase respectively. r , L_s , and M are resistance, inductance and mutual inductance of the stator winding respectively. Rotor angular speed can be presented as

$$\omega_r = \frac{d\theta_r}{dt} \quad (2)$$

where θ_r is the rotor electrical angle. The electromagnetic torque in terms of the back-EMFs and currents per phase, and the speed can be expressed as

$$T_e = T_{ea} + T_{eb} + T_{ec} = \frac{e_a i_a + e_b i_b + e_c i_c}{\omega_m} \quad (3)$$

where T_{ea} , T_{eb} and T_{ec} are the electromagnetic torque of phase A, B, and C, respectively. The electromagnetic torque is proportional to the back-EMF and its corresponding current, hence the phase currents are automatically shaped to achieve the desired electromagnetic torque characteristics using Eq. (3). When back-EMF constant waveforms from the pre-stored look-up table in the actual stationary reference frame are used in Eq. (3), electromagnetic torque smooth more and more as shown in Fig. 1.

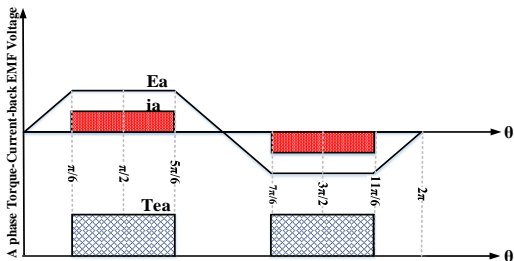


Fig. 1. Back EMF, current and torque of phase A.

Fig. 2 shows the connections of the drive with two phases (phase-A and phase-B) of the BLDC motor supplied through the inverter legs, while the third one (phase-C) is linked to the middle point of the dc-bus

voltage.

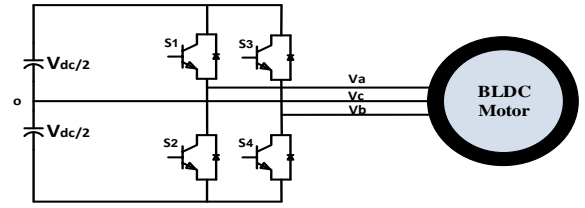


Fig. 2. BLDC motor drives fed by four-switch inverters.

3. THE PROPOSED FOUR-SWITCH DPC OF BLDC MOTOR DRIVE

In this section proposed control method for BLDC motor drive is presented.

3.1. Formulation

The key issue in the proposed four-switch DPC of a BLDC motor drive is to correct calculation of the power. The input electrical power is the same as the electromagnetic power if the stator winding loss and core loss are small enough to be neglected. The electrical input power can be approximated as the mechanical output power and can be expressed as

$$P_{in} \cong P_e \cong P_{out} \quad (4)$$

where P_{in} , P_e and P_{out} represent the electrical input power, the electromagnetic power, and the mechanical output power, respectively. The mechanical input power can be presented as

$$P_{in} = T_{em} \frac{\omega_r}{p} \quad (5)$$

In order to the simplicity of BLDC analysis and control, reference frame theory is used in Ref. [29]. Using this theory complexities of the time-varying inductances are purposely omitted. The transformation the arbitrary reference frame to stationary reference frame is shown in Fig. 3. So the electromagnetic torque of a BLDC motor in the synchronously rotating dq reference frame can be expressed as [28], [30].

$$T_{em} = \left(\frac{3}{2}\right) \left(\frac{p}{2}\right) \left[\begin{aligned} &\left(\frac{dL_{ds}}{d\theta_e} i_{sd} + \frac{d\varphi_{dr}}{d\theta_e} - \varphi_{sq} \right) i_{sd} + \\ &\left(\frac{dL_{qs}}{d\theta_e} i_{sq} + \frac{d\varphi_{qr}}{d\theta_e} + \varphi_{sd} \right) i_{sq} \end{aligned} \right] \quad (6)$$

Substitution of the torque from Eq. 5 into Eq. 6 result the following as

$$P_{out} = \frac{3\omega_r}{4} \left[\begin{aligned} &\left(\frac{dL_{ds}}{d\theta_e} i_{sd} + \frac{d\varphi_{dr}}{d\theta_e} - \varphi_{sq} \right) i_{sd} + \\ &\left(\frac{dL_{qs}}{d\theta_e} i_{sq} + \frac{d\varphi_{qr}}{d\theta_e} + \varphi_{sd} \right) i_{sq} \end{aligned} \right] \quad (7)$$

where θ_e is the angle between α -axis in $\alpha\beta$ stationary reference frame and d-axis in dq synchronous

reference fram as shown in Fig. 3. p is the number of poles, i_{sd} and i_{sq} are d and q-axes currents, L_{ds} and L_{qs} are d and q-axes stator inductances, and φ_{rd} , φ_{rq} , φ_{sd} , and φ_{sq} are d and q-axes rotor and stator flux linkages, respectively. If L_{ds} and L_{qs} are considered to be constant, Eq. (6) can be rewritten as

$$P_{out} = \frac{3\omega_r}{4} \begin{bmatrix} \left(\frac{d\varphi_{dr}}{d\theta_e} - \varphi_{sq} \right) i_{sd} + \\ \left(\frac{d\varphi_{qr}}{d\theta_e} + \varphi_{sd} \right) i_{sq} + \\ (L_{qs} - L_{ds}) i_{sd} i_{sq} \end{bmatrix} \quad (8)$$

For the non-salient-pole rotor is:

$$L_{sd} = L_{sq} \quad (9)$$

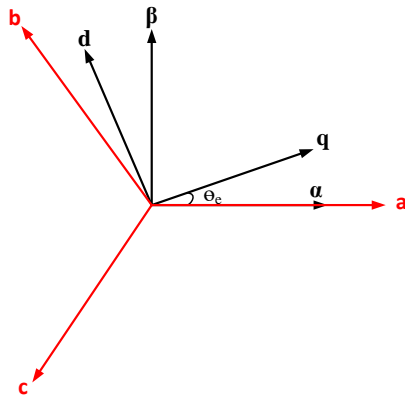


Fig. 3. Inverse Park transformation.

The flux linkages and stator currents in the stationary $\alpha\beta$ reference frame, can be given as

$$\varphi_{r\alpha} = \varphi_{rd} \cos \theta_e - \varphi_{rq} \sin \theta_e \quad (10)$$

$$\varphi_{r\beta} = \varphi_{rd} \sin \theta_e + \varphi_{rq} \cos \theta_e \quad (11)$$

$$i_{s\alpha} = i_{sd} \cos \theta_e - i_{sq} \sin \theta_e \quad (12)$$

$$i_{s\beta} = i_{sd} \sin \theta_e + i_{sq} \cos \theta_e \quad (13)$$

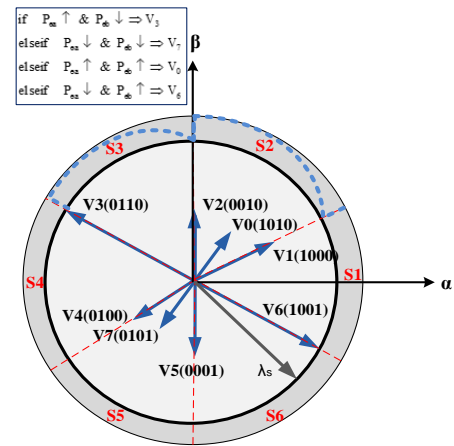
The power equation can be simplified as

$$P_{out} = -\frac{3}{2} \frac{\omega_r}{2} \left[\frac{d\varphi_{r\alpha}}{d\theta_e} i_{s\alpha} + \frac{d\varphi_{r\beta}}{d\theta_e} i_{s\beta} \right] = -\frac{3}{2} \frac{\omega_r}{2} \left[\frac{e_\alpha}{\omega_e} i_{s\alpha} + \frac{e_\beta}{\omega_e} i_{s\beta} \right] \quad (14)$$

where, e_α and e_β are back-EMF derived from the look up table. In BLDC motor, only two phase powers are involved in the total power equation during every 60° electrical and the other phase power will be equal zero as shown in Table 1. The total power of BLDC motors equals the sum of each phase power which is given as

$$P_{em} = P_{ea} + P_{eb} + P_{ec} \quad (15)$$

As it has been shown in Fig. 4, for stator flux linkage trajectory, when conventional two-phase four-switch PWM current control is used sharp dips occur every 60° electrical. This is due to freewheeling diodes. The same phenomenon has been noticed when the DPC strategy for a BLDC motor is used, as shown in Fig. 4. Due to the sharp dips in the stator linkage flux space vector at every commutation (60° electrical) and the tendency of the currents to match with the flat top portion of the phase back-EMF for smoothing torque generation, there is no easy way to control the stator linkage flux amplitude. On the other hand, the rotational speed of the stator linkage flux can be easily controlled, so fast torque response can be obtained. The size of the sharp dips is quite unpredictable and depends on several factors such as sampling time, motor parameters especially the winding inductance, hysteresis bandwidth, dc-link voltage, motor speed, snubber circuit, and the amount of load torque. The best way to control the amplitude is to know the exact shape of stator linkage flux, but it needs cumbersome process in the constant torque region. In the two-phase four-switch DPC of the BLDC motor drive, the flux error in the look-up table voltage vector is always selected zero and only the power error is used depending on the error level of the actual power from the reference power.



$$V_1=V_2=V_4=V_5=V_{dc}/2$$

$$V_3=V_6=V_{dc} \quad V_0=V_7=V_{dc}/3$$

Fig. 4. Switching vector for four-switch DPC inverter in $\alpha\beta$ stationary frame.

Table 1. Electromagnetic power in eight sector.

For $(330^\circ < \theta_e < 30^\circ)$	$P_{em} = P_{eb} + P_{ec} \ \& \ P_{ea} = 0$
For $(30^\circ < \theta_e < 90^\circ)$	$P_{em} = P_{ea} + P_{eb} \ \& \ P_{ec} = 0$
For $(90^\circ < \theta_e < 150^\circ)$	$P_{em} = P_{ea} + P_{ec} \ \& \ P_{eb} = 0$
For $(150^\circ < \theta_e < 210^\circ)$	$P_{em} = P_{eb} + P_{ec} \ \& \ P_{ea} = 0$
For $(210^\circ < \theta_e < 270^\circ)$	$P_{em} = P_{ea} + P_{eb} \ \& \ P_{ec} = 0$
For $(270^\circ < \theta_e < 330^\circ)$	$P_{em} = P_{ea} + P_{ec} \ \& \ P_{eb} = 0$

3.2. Control of power by selecting the proper stator voltage space vector

To calculate the six modes of operation in four-switch DPC of BLDC motor drive, a simple voltage vector selection look-up table is designed as shown in Table 2. Normally, six-possible voltage space vectors of four-switch topology are supposed to be used in Table 2 as shown in Fig. 5(a)–(f) similar to the six-switch version. However, two of the voltage vectors V3 and V6 as shown in Fig. 5 create problems in the power control. When they are directly used in the voltage vector selection table (Table 2), back-EMF of the uncontrolled phase (phase-c) generates undesired current; therefore distortions occur in each phase power. As a result, undesired power is inevitable. Therefore, when the rotor position is in the Sector II and V, special switching pattern should be adapted, as shown in Table 3 (CCW). At Sectors II and V, phase-a and phase-b power are independently controlled by the hysteresis power controllers. Additional two voltage vectors V0 and V7, which are used in conventional four-switch PWM scheme are included in the voltage selection look-up table to obtain smooth power production in two-phase four-switch DPC of BLDC motor drive. Since the upper and lower switches in a phase leg may be simultaneously off, irrespective of the state of the associated freewheeling diodes in two-phase conduction mode, four digits are required for the four-switch inverter operation, one digit for each switch. Therefore, there is a set of eight digits useful voltage vectors for the two-phase conduction mode in the proposed DPC of BLDC motor drive which can be represented as V0,1,2,...,6,7 (SW1, SW2, SW3, SW4), as shown in Fig. 4. The eight possible two-phase four-switch voltage vectors and current flow are depicted in Fig. 5. The detailed switching sequence and power regulation are shown in Fig. 6 for four-switch DPC of BLDC motor drive. The overall block diagram of the closed-loop four-switch DPC scheme of a BLDC motor drive in the constant torque region is represented in Fig. 7. In the two-phase conduction mode, the shape of stator flux linkage trajectory is ideally expected to be hexagonal. However, the influence of the unexcited open-phase back-EMF causes that each straight side of the ideal hexagonal shape of the stator flux linkage locus to be curved. Therefore, the actual stator flux linkage trajectory tends to be more circular in shape. Similar to DTC method, switching frequency of the proposed strategy is variable. Frequency switching is dependence on two hysteresis based comparators which modify the switching logic according to the errors of power and flux. In general, a smaller power hysteresis band results

in smaller power ripples and higher switching frequency.

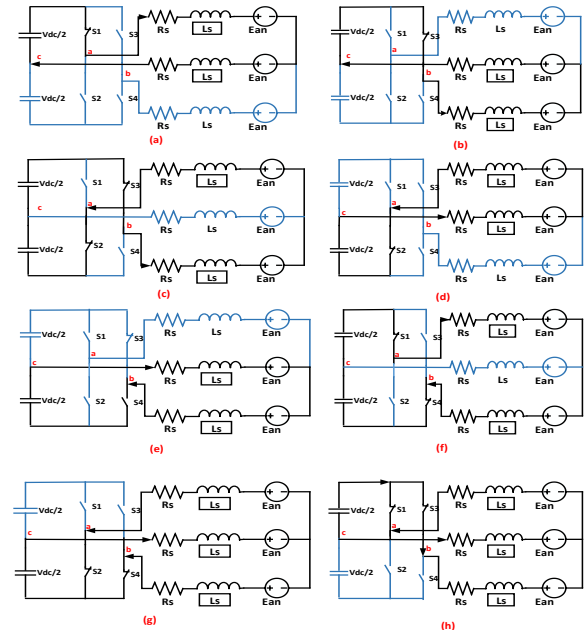


Fig. 5. Eight-possible voltage space vectors of four-switch inverter

Table 2. Voltage vector selection look-up table.

Power error	Rotor angular position sector					
	θ_1	θ_2	θ_3	θ_4	θ_5	θ_6
1	V2 (0010)	V3 (0110)	V4 (0100)	V5 (0001)	V6 (1001)	V1 (1000)
-1	V5 (0001)	V6 (1001)	V1 (1000)	V2 (0010)	V3 (0110)	V4 (0100)

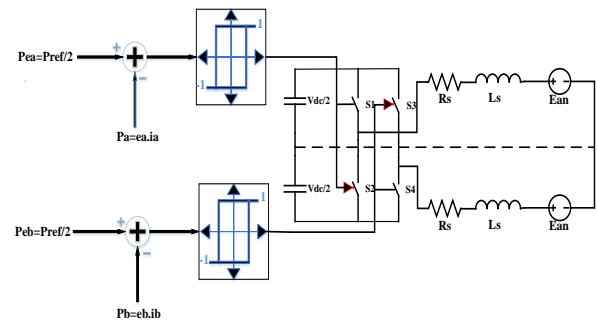


Fig. 6. The detailed switching sequence and power regulation for four-switch DPC of BLDC motor drive

Table 3. Special switching pattern for rotor position in the sector 2 and 5.

P _{ea}	P _{eb}	Rotor angular position sector	
		θ_2	θ_5
1	1	V3(0110)	V6 (1001)
	-1	V7(0101)	V0(1010)
-1	1	V0(1010)	V7(0101)
	-1	V6 (1001)	V3(0110)

The overall block diagram of the proposed closed-loop four-switch DPC strategy of BLDC motor drive in the constant torque region.

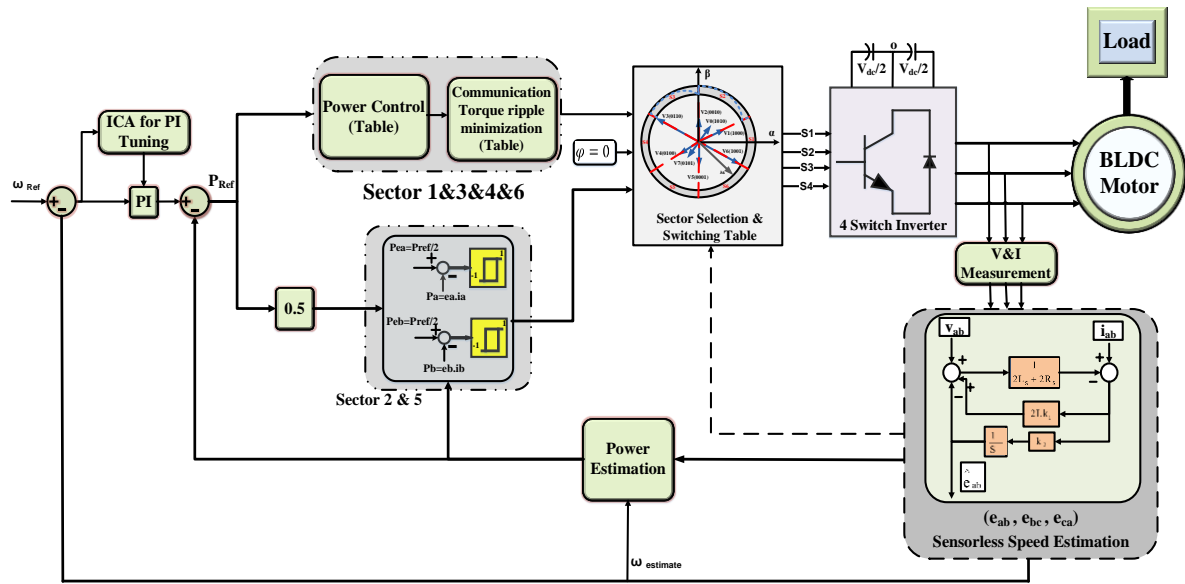


Fig. 7. The overall block diagram of the proposed closed-loop four-switch DPC strategy of BLDC motor drive in the constant torque

3.3. Proposed commutations ripple minimization

This paper proposed a new DPC strategy in which a capability of reducing the torque ripple during sector to sector commutations is presented. The proposed method is an approach consisting in the application of active voltage vectors corresponding to the two-phase conduction mode, at the beginning of each sector in order to force the current in the turned-off phase to flow through a controllable IGBT instead of an uncontrollable freewheeling diode. Thus, the rising rate (di/dt) of the current in the turned-off phase is regulated to make it similar to the one of the current in the turned-on phase. It consists in the substitution of the two-level power controller by a four-level one. In fact, the positive high level ($P_e = +2$) of the power hysteresis controller is systematically activated when the power falls during sector to sector commutations in the case of an anticlockwise rotation ($P_e > 0$), whereas its negative high level ($P_e = -2$) is systematically activated when the power falls during sector to sector commutations in the case of a clockwise rotation ($P_e < 0$). The low levels ($P_e = \pm 1$) are applied during the whole cycle except for the power dips taking place during sector to sector commutations. As mentioned, the proposed DPC strategy presents a capability of reducing the torque ripple during sector-to-sector commutations without any dependence of motor and inverter parameters. The proposed vector selection sub tables are provided in Tables 4 and 5, respectively. Accounting for the reference phase currents shown in Fig. 1, it should be underlined that the proposed approach is useless during the commutations from Sector1 to Sector-2 and from Sector-4 to Sector-5 in the case of an anticlockwise rotation, and from

Sector III to Sector II and from Sector VI to Sector V in the case of a clockwise rotation, due to the fact that $|di_c/dt|$ is uncontrollable. As mentioned, the proposed DPC strategy presents a capability of reducing the torque ripple during sector-to-sector commutations without any dependence of motor and inverter parameters.

Table 4. Vector selection sub table during sector to sector commutations in case anticlockwise rotation.

P_e	2
T_o Sector VI \rightarrow Sector I	V0(1010)
T_o Sector II \rightarrow Sector III	V3(0110)
T_o Sector III \rightarrow Sector IV	V7(0101)
T_o Sector V \rightarrow Sector VI	V6(1001)

Table 5. Vector selection sub table during sector to sector commutations in case anticlockwise rotation.

P_e	2
T_o Sector II \rightarrow Sector I	V6(1001)
T_o Sector I \rightarrow Sector VI	V7(0101)
T_o Sector V \rightarrow Sector IV	V3(0110)
T_o Sector IV \rightarrow Sector III	V0(1010)

The implementation of the proposed method is shown in Fig.7.

3.4. Sensorless control method

The In this section, the sensorless method used to estimate the speed is presented. An unknown input observer uses a back-EMF as an unknown input and state of the BLDC motor drive. This strategy can be explained as follows; the unknown input observer can be expressed by the following line-to-line equation as

$$\frac{di_{ab}}{dt} = -\frac{2R_s}{2L}i_{ab} + \frac{1}{2L}v_{ab} - \frac{1}{2L}e_{ab} \tag{16}$$

where i_{ab} and v_{ab} are “known” state variables because they can be measured. e_{ab} is “unknown” state because it cannot be able to measurement. Eq. (16) can be rewritten as

$$\frac{dx}{dt} = Ax + Bu + Fw \tag{17}$$

$$y = Cx \tag{18}$$

where $A = \begin{bmatrix} -\frac{2R_s}{2L} \end{bmatrix}$, $B = \begin{bmatrix} \frac{1}{2L} \end{bmatrix}$, $F = \begin{bmatrix} -\frac{1}{2L} \end{bmatrix}$ and

$x = [i_{ab}]$, $u = [v_{ab}]$, $w = [e_{ab}]$, $y = [i_{ab}]$, $C = [1]$. The back-EMF is regarded as an unknown disturbance and can be given as

$$\frac{dz}{dt} = Dz \tag{19}$$

$$w = Hz \tag{20}$$

where H and D can be presented as

$$D = \begin{bmatrix} 0 & I \\ 0 & 0 \end{bmatrix}, H = [I \quad 0] \tag{21}$$

δ is degree of polynomial and I is identity matrix δ expression under:

$$w = \sum_{i=0}^{\delta} a_i t^i, \quad \delta \geq 1 \tag{22}$$

where a_i denotes a set of unknown coefficient vectors. Because of no experimental information about disturbance, a_i can be defined as $a_i = 0$ in Eq. (22). So the augmented equation observer can express the all of system and introduces disturbances with differential equation form modeling the back-EMF. The augmented model can be given as

$$\frac{dx_a}{dt} = A_a x_a + B_a u \tag{23}$$

$$y = C_a x_a \tag{24}$$

where

$$A_a = \begin{bmatrix} -\frac{2R_s}{2L} & -\frac{1}{2L} \\ 0 & 0 \end{bmatrix}, B_a = \begin{bmatrix} \frac{1}{2L} \\ 0 \end{bmatrix}, C_a = [1 \quad 0], x_a = \begin{bmatrix} i_{ab} \\ e_{ab} \end{bmatrix}, u = [v_{ab}], y = [i_{ab}]$$

The degree of polynomial expression for disturbance is extracted by $\delta = 1$. Whereas systems of Eq. (23) And Eq. (25) are observable, it is possible to compose the

following observer:

$$\frac{d\tilde{x}_a}{dt} = A_a \tilde{x}_a + B_a u + K (y - \tilde{y}) \tag{25}$$

K is the gain matrix. The observer can accurately estimate line-to-line currents and back-EMF of motors when the gain of the observer is selected properly. Block diagram of the presented back-EMF observer has been shown in Fig. 7.

3.5. Speed controller design for reference tracking

As shown in the Fig 6, the classic controller is used to track the reference speed. There are various methods for tuning the controller parameters. In this paper, an imperialist Competition Algorithm is illustrated to design PI controller for speed and torque control.

3.5.1. Optimization algorithm

ICA has been designed by the imperialistic competition for optimization. Like other optimization algorithms, ICA starts with an initial population. Every population is a country which has two types: imperialists and colonies with together compose some empires. Imperialistic competition among these empires forms the basis of the evolutionary algorithm. During the competition, powerful empires take possession of their colonies and weak empires collapse. Imperialistic competition hopefully converges to a state in which there exists only one empire and its colonies have the same cost as the imperialist and colonies are in the same position [24], [31].

Fig. 8 shows the movement of a colony towards the relevant imperialist. In this movement, α and x are random numbers with uniform distribution and d is the distance between colony and the imperialist.

$$\begin{aligned} x &\sim U(0, \alpha \times d) \\ \alpha &\sim U(-\gamma, \gamma) \end{aligned} \tag{26}$$

In Eq. (26) α and γ are arbitrary numbers that modify the area that colonies randomly search around the imperialist.

Initial number of countries is set at 100, twelve of which are chosen as the initial imperialists in the ICA. The maximum number of iterations of the ICA is set at 90.

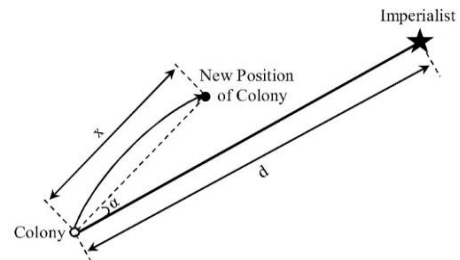


Fig. 8. Motion of colonies toward their relevant imperialist.

3.5.2. Objective function

In this paper, the sum of the sample values in the discrete Fourier transform called samples magnitude values sum in discrete Fourier transform (SMVS-DFT) of speed and torque deviations to their reference values are used as the objective function. This function is referred to as SMVS-DFT in [32]. Therefore, the objective function to optimize PI controllers' parameters for four-switch two-phase DPC control BLDC is expressed as

$$f_{objective} = SMVS_DFT(\omega_r - \omega_{ref}) + SMVS_DFT(T_{em} - T_{ref}) \quad (27)$$

The weight coefficients in the equation of the objective function with respect to the maximum deviation of the variables in the optimum mode have been selected using the trial and error method and the observation of the amount of deviation of the mentioned variables from the reference values in the simulation. Also in the SMVS-DFT function, all control variable samples measured in a controlled time range are given to a target function, the SMVS-DFT function obtains the fast Fourier transform of the given samples from the zero-to-highest desired harmonic that is here (sampling frequency/2). Then the SMVS-DFT function collects the obtained harmonic magnitude and returns the resulting value as the cost function to the optimization algorithm [32]. The sampling frequency is obtained from the following equation:

$$Sampling\ frequency = 1 / (sampling\ time) \quad (28)$$

$$Sampling\ time = 1 / (rated\ frequency * (sample\ per\ cycle) - 1) \quad (29)$$

4. SIMULATION RESULTS

In this section, the superiority of the proposed method and the simulation results is presented. The simulation is implemented in MATLAB/SIMULINK® and it is carried out according to Fig. 7 block diagram that aims the speed control of motor. The parameters used for simulation is presented in Appendix 1.

The proposed PI speed controller parameters have been optimized through ICA. To optimize these parameters, firstly initial controller parameters are selected using the ICA and then the simulation process is executed. After the simulation, the values of the objective function are calculated and this process continues until the objective function is optimized. Fig. 9 shows the optimization process and increasing the objective function. Also, Fig. 10 shows the powerful empire and its colonies after the optimization process is done. As can be seen in this figure, the powerful empire is very big because it has a minimum objective function.

Also, the figure shows that the other empires have been lost.

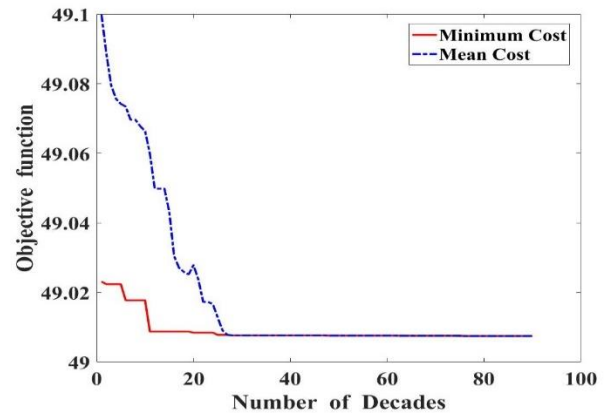


Fig. 9. The process of reducing the objective function.

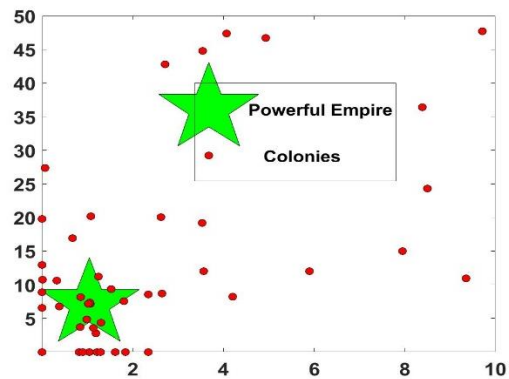


Fig. 10. The powerful empire and its colonies after the optimization process.

Based on the controller parameters witch obtained from previous section, the Bode diagram of the control system is extracted. Transfer function of BLDC motor along with controller can be given by [33]:

$$G_u(s) = \frac{\omega(s)}{V(s)} = \frac{k_T}{L_s J s^2 + (rJ + L_s B_v) s + (rB_v + k_e k_T)} \left(k_p + \frac{k_i}{s} \right) \quad (30)$$

where B_v is viscous friction coefficient, J is moment of inertia, k_T is torque coefficient, k_e is coefficient of line back-EMF, k_i is integral coefficient, and k_p is proportional gain. The open loop analysis is done by considering the stability factors and is made Bode plot diagram for the open loop transfer function $G_u(s)$. This plot is presented in Fig. 11 which phase margin is 70° . Therefore, close loop speed loop is stable. Therefore, both controllers are stable systems

4.1. Validation of torque dips minimization

In the first case, the proposed method has been used

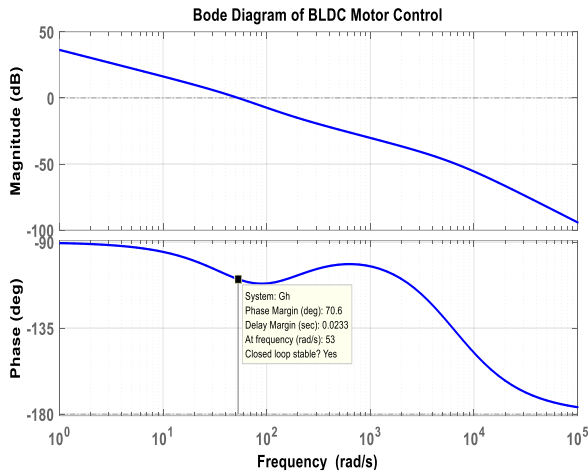


Fig. 11. Bode plot diagram of the BLDC motor along with controller.

motor is presented in Fig. 12. As can be seen in Fig. 12, the torque has ripple under sector to sector commutation. The torque of the motor is shown in the Fig. 13 while a method of ripple torque reduction based on changing sectors has been used. According to the figure, the proposed method (changing sectors method) decreases the torque ripple. Reducing the torque ripple improves motor performance and reduces noise.

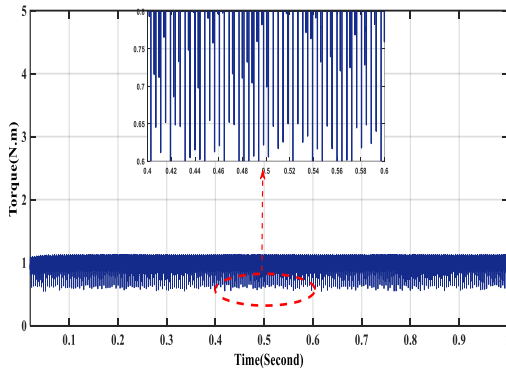


Fig. 12. The torque of the motor without ripple torque reduction method.

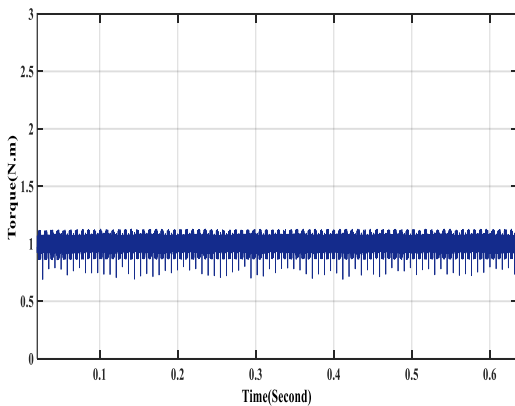


Fig. 13. The torque of the BLDC motor with ripple torque reduction method.

equations should be numbered serially throughout the paper. The equation number should be located to the far

right of the line in parenthesis. Equations are shown left aligned on the column.

4.2. BLDC motor speed estimating using presented sensorless method

The performance of the sensorless method is evaluated for a period of 2 s. As the second test case, the estimated speed and actual speed of BLDC motor under variation of the reference are presented. The speed reference is changed to 140 rad/s at $t = 0.5$ s and the motor torque is increased at $t = 1$ s. As shown in Fig. 14, it is clear that the motor speed is accurately estimated using a sensorless method and the motor speed is well-estimated at $t = 0.5$ s and $t = 1$ s.

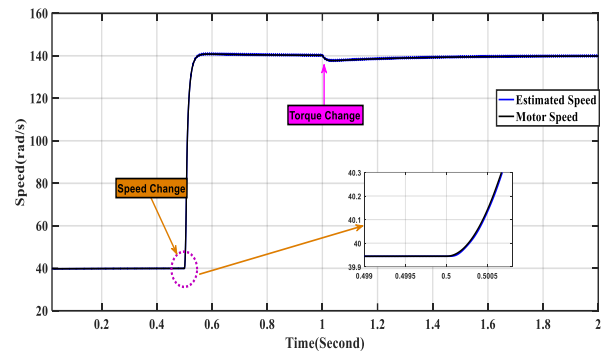


Fig. 14. The speed of the BLDC motor.

4.3. Tracking the Speed using proposed method

In this section, simulations are carried out for a step change of speed when DPC method is used. From Fig. 15, it is plain that with the proposed method, the motor follows the reference speed truly. Back-EMF for step change of speed is shown in Fig. 16. It is clear that as the speed increases, the back-EMF increases.

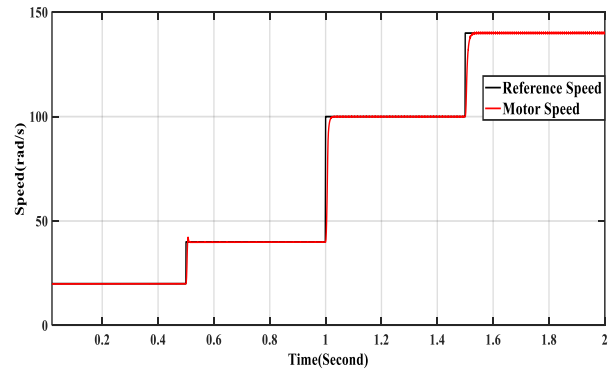


Fig. 15. Step change of motor speed.

4.1. Tracking the torque

As the fourth test case, the motor speed is fixed and the torque increases. Fig. 17 shows the step change of motor torque. The motor three phase currents are shown in Fig. 18. Increasing the amount of torque increases the motor current rate. It is clear that all three phases of the motor drive the symmetrical current. According to the simulation results, it is clear that the proposed method has acceptable responses for different motor situations.

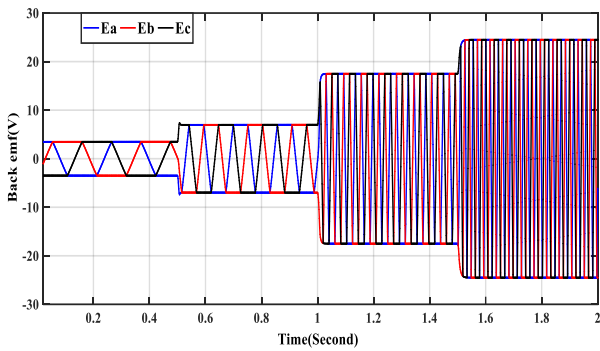


Fig. 16. Motor back-EMF for step change of speed with DPC method.

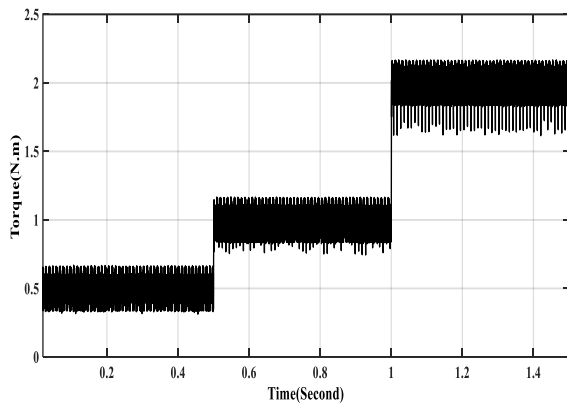


Fig. 17. Motor torque for step change of torque.

4.2. Tracking the Speed using proposed method

In order to evaluate the performance of the proposed method, this strategy is compared with the DTC method which presented in [8].

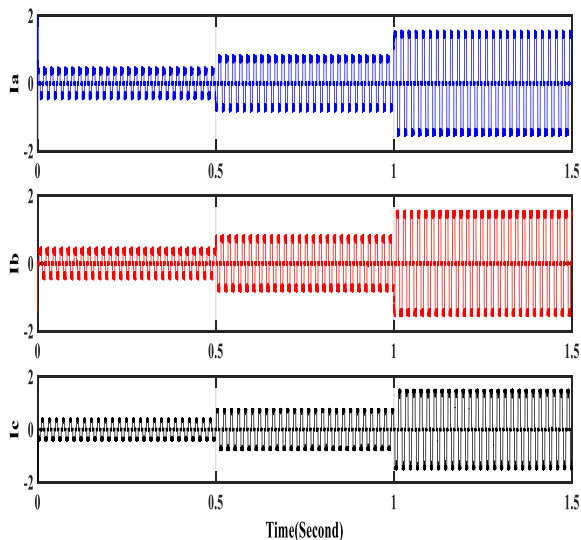


Fig. 18. Motor current for step change of torque.

The proposed ripple reduction method is applied to both DTC and DPC control strategy. Fig. 19 shows the torque comparison of the proposed method and the DTC method. In the same conditions, the power estimation is

faster than torque estimation, therefore, the dynamic response of the DPC method is faster than the DTC method, as seen in Fig.19. One of the major advantages of the DPC method compared to the DTC method that it is can be easily estimated actual power for control system. The comparison of the motor speed for both methods is presented in Fig. 20. It can be seen, the response of speed tracking is good and acceptable in both methods. However, the rise time in the DPC method is shorter than the DTC method.

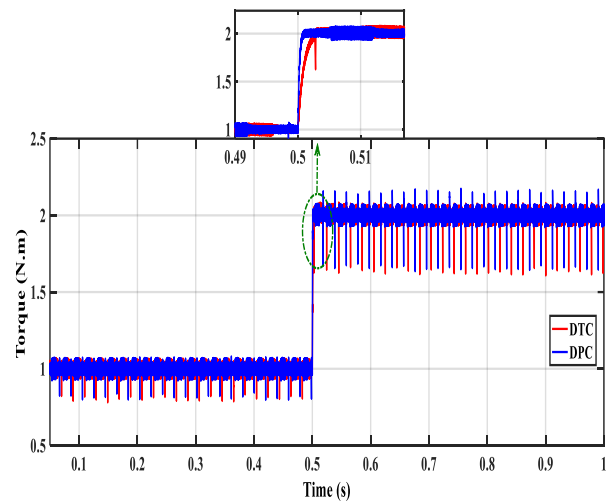


Fig. 19. Motor electromagnetic torque in DTC and DPC control methods

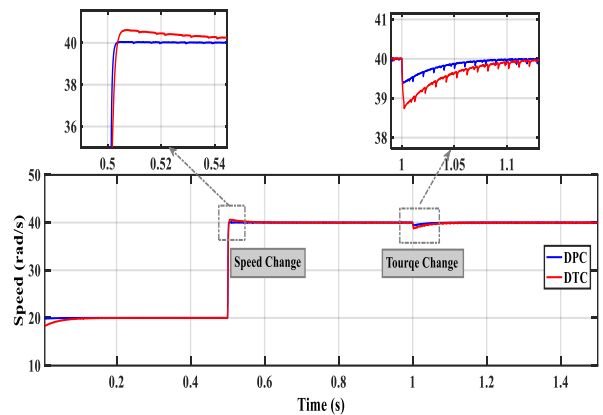


Fig. 20. Comparison of speed in DTC and DPC control methods

5. CONCLUSIONS

In this paper, BLDC motor control with 4 switches inverter and power direct control method for BLDC motor control in constant flux region is implemented. Using 4 switches inverter in the proposed method, the price of drive and switching losses is reduced. According to the simulations, it is shown that the proposed method is suitable and efficient. As the proposed method uses the power feedback, its

implementation is more convenient. One of the major advantages of the DPC method compared to the DTC method is that the actual power for the control system can be easily estimated. Compared to the three-phase DPC technique, this approach eliminates the flux control and only torque was considered in the overall control system. Simulations have been done for various modes of operations using MATLAB/SIMULINK[®] software. According to the results, DPC method is an effective and practical method for BLDC motors control. Load and speed changes are the most important issues in the control of BLDC motors that were checked for proposed control method, and it is clear that the proposed control method has a good and proper performance against these changes. The power control is a promising method since it can be extended to others machine topologies with non-sinusoidal back-EMF such as interior permanent magnet synchronous motors and synchronous reluctance motors.

Appendix A.

The specifications of the BLDC motor chosen for simulation are presented in Table. A.

Table A. BLDC motor parameters.

Parameters	index	Values
Number of poles	P	4
Rated speed	ω_{rated}	1500 rpm
DC link voltage	V_{dc}	300 V
Stator inductance	L_s	1mH
Stator resistance	R_s	0.4 ohm
Damping coefficient	B	0.002 N.m/rad/s
inertia	J	0.004 kg.m ²
Load torque	C	3 N.m
Linkage flux	λ_m	0.175 V.s

REFERENCES

- [1] J. Gromba, "Torque control of BLDC motor for electric bicycle," *2018 Int. Sym. Electr. Mach. (SME)*, 2018, pp. 1-5.
- [2] M. Jagiela, T. Garbiec, J. Gwozdz and J. Kolodziej, "Fast steady-state field-circuit model for SMPM-BLDC motors driven from 120° and 180° quasi-square wave inverters," *IEEE Trans. Magn.*, vol. 52, no. 3, pp. 1-4, Mar. 2016.
- [3] H. K. Samitha Ransara and U. K. Madawala, "A torque ripple compensation technique for a low-cost brushless dc motor drive," *IEEE Trans. Ind. Electron.*, vol. 62, no. 10, pp. 6171-6182, Oct. 2015.
- [4] M. Masmoudi, B. El Badsı and A. Masmoudi, "Direct torque control of brushless dc motor drives with improved reliability," *IEEE Trans. Ind. Appl.*, vol. 50, no. 6, pp. 3744-3753, Nov. 2014.
- [5] W. Li, J. Fang, H. Li and J. Tang, "Position sensorless control without phase shifter for high-speed bldc motors with low inductance and nonideal back emf," *IEEE Trans. Power Electron.*, vol. 31, no. 2, pp. 1354-1366, Feb. 2016.
- [6] M. Baszynski and S. Pirog, "Unipolar modulation for a BLDC motor with simultaneously switching of two transistors with closed loop control for four-quadrant operation," *IEEE Trans. Ind. Inf.*, vol. 14, no. 1, pp. 146-155, Jan. 2018.
- [7] M. Moazen and M. Sabahi, "Electric differential for an electric vehicle with four independent driven motors and four wheels steering ability using improved fictitious master synchronization strategy," *J. Oper. Authom Power Eng.*, vol. 2, no. 2, pp. 141-150, 2014.
- [8] S. B. Ozturk, W. C. Alexander, and H. A. Toliyat, "Direct torque control of four-switch brushless dc motor with non-sinusoidal back EMF," *IEEE Trans. Power Electron.*, vol. 25, no. 2, pp. 263-271, 2010.
- [9] A. G. de Castro, W. C. A. Pereira, T. E. P. de Almeida, C. M. R. de Oliveira, J. Roberto Boffino de Almeida Monteiro, and A. A. de Oliveira, "Improved finite control-set model-based direct power control of BLDC motor with reduced torque ripple," *IEEE Trans. Ind. Appl.*, vol. 54, no. 5, pp. 4476-4484, Sep. 2018.
- [10] C. K. Lad and R. Chudamani, "Simple overlap angle control strategy for commutation torque ripple minimisation in BLDC motor drive," *IET Electr. Power Appl.*, vol. 12, no. 6, pp. 797-807, Jul. 2018.
- [11] J. E. MuraliDhar and P. Varanasi, "A progressive rugged appearance of fuzzy controller fed four-switch BLDC drive," *Procedia Comput. Sci.*, vol. 47, pp. 144-152, 2015.
- [12] B. Abdi, M. M. Teymoori, H. Gholamrezaei and A. A. Nasiri, "A simple analog BLDC drive control for electro-mechanical energy storage system," *Energy Proce.*, vol. 12, pp. 1002-1007, 2011.
- [13] B. K. Lee and M. Ehsani, "Advanced BLDC motor drive for low cost and high performance propulsion system in electric and hybrid vehicles," *IEMDC 2001. IEEE Int. Electr. Mach. Drives Conf. (Cat. No.01EX485)*, pp. 246-251.
- [14] M. S. Aspalli, F. M. Munshi and S. L. Medegar, "Speed control of BLDC motor with four switch three phase inverter using digital signal controller," *2015 Int. Conf. Power Adv. Control Eng.*, 2015, pp. 371-376.
- [15] S. Hajiaghahi, A. Salemnia, and F. Motabarian, "Four switches direct power control of BLDC motor with trapezoidal back-EMF," *2017 8th Power Electron. Drive Syst. Technol. Conf.*, 2017, pp. 513-518.
- [16] S. Ogasawara and H. Akagi, "An approach to position sensorless drive for brushless DC motors," *IEEE Trans. Ind. Appl.*, vol. 27, no. 5, pp. 928-933, 1991.
- [17] J. C. Moreira, "Indirect sensing for rotor flux position of permanent magnet AC motors operating over a wide speed range," *IEEE Trans. Ind. Appl.*, vol. 32, no. 6, pp. 1394-1401, 1996.
- [18] J. X. Shen, Z. Q. Zhu and D. Howe, "Sensorless flux-weakening control of permanent-magnet brushless machines using third harmonic back EMF," *IEEE Trans. Ind. Appl.*, vol. 40, no. 6, pp. 1629-1636, 2004.
- [19] T. M. Jahns, R. C. Becerra and M. Ehsani, "Integrated current regulation for a brushless ECM drive," *IEEE Trans. Power Electron.*, vol. 6, no. 1, pp. 118-126, 1991.
- [20] G.-J. Su and J. W. McKeever, "Low-Cost sensorless control of brushless dc motors with improved speed range," *IEEE Trans. Power Electron.*, vol. 19, no. 2, pp. 296-302, 2004.
- [21] S.-H. Huh, S.-J. Seo, I. Choy and G.-T. Park, "Design of a robust stable flux observer for induction motors," *J. Electr. Eng. Technol.*, vol. 2, no. 2, pp. 280-285, 2007.
- [22] M. H. Sureshjani, "An improved direct torque control for torque ripple minimization of four-switch brushless dc

- motor with trapezoidal back-emf," *20th Iran. Conf. Electr. Eng.*, 2009.
- [23] G. Jiang, C. Xia, W. Chen, T. Shi, X. Li and Y. Cao, "Commutation torque ripple suppression strategy for brushless dc motors with a novel noninductive boost front end," *IEEE Trans. Power Electron.*, vol. 33, no. 5, pp. 4274-4284, 2018.
- [24] V. Viswanathan and J. Seenithangom, "Commutation torque ripple reduction in the BLDC motor using modified SEPIC and three-level NPC inverter," *IEEE Trans. Power Electron.*, vol. 33, no. 1, pp. 535-546, 2018.
- [25] Z. Zeng, C. Zhu, X. Jin, W. Shi and R. Zhao, "Hybrid space vector modulation strategy for torque ripple minimization in three-phase four-switch inverter-fed pmsm drives," *IEEE Trans. Ind. Electron.*, vol. 64, no. 3, pp. 2122-2134, 2017.
- [26] M. Masmoudi, B. El Badsı and A. Masmoudi, "DTC of B4-inverter-fed BLDC motor drives with reduced torque ripple during sector-to-sector commutations," *IEEE Trans. Power Electron.*, vol. 29, no. 9, pp. 4855-4865, 2014.
- [27] A. Nafar, G. R. Arab Markadeh, A. Elahi and R. Pouraghababa, "Low voltage ride through enhancement based on improved direct power control of DFIG under unbalanced and harmonically distorted grid voltage," *J. Oper. Autom. Power Eng.*, vol. 4, no. 1, pp. 16-28, Jun. 2016.
- [28] A. Halvaei Niasar and M. Behzadi Shahrabak, "Direct power control of brushless DC generator for automotive applications," *Proce. 5th Annu. Int. Power Electron., Drive Syst. Technol. Conf.*, 2014, pp. 267-272.
- [29] P. C. Krause, O. Wasynczuk, S. D. Sudhoff and P. C. Krause, *Analysis Electr. Mach. Drive Syst.*, IEEE Press, 2002.
- [30] P. Devendra, C. P. Kalyan, K. A. Mary, and Ch. Saibabu, "Simulation approach for torque ripple minimization of BLDC motor using direct torque control," *Int. J. Adv. Res. Electr. Electron. Instrum. Energy*, vol. 2, no. 8, pp. 3703-3710.
- [31] E. Atashpaz-Gargari and C. Lucas, "Imperialist competitive algorithm: An algorithm for optimization inspired by imperialistic competition," *Proce. 2007 IEEE Congr. Evol. Comput.*, 2007, pp. 4661-4667.
- [32] Z. Rafiee, A. F. Meyabadi and H. Heydari, "PSS parameters values finding using SMVSDFT objective function and a new technique for multi-objective function in a multi-machine power system," *Int. J. Power Energy Convers.*, vol. 6, no. 3, 2015.
- [33] K. Sugano, *Permanent Magnet Brushless DC Motor Drives and Controls*. Wiley-Blackwell, 2012.